



Research Report

Altered effective connectivity between lateral occipital cortex and superior parietal lobule contributes to manipulability-related modulation of the Ebbinghaus illusion



Lihong Chen^{a,b,c,*}, Shengnan Zhu^{a,b}, Bengang Feng^{a,b}, Xue Zhang^c and Yi Jiang^{c,d,e,f,**}

^a Research Center of Brain and Cognitive Neuroscience, Liaoning Normal University, Dalian, PR China

^b Key Laboratory of Brain and Cognitive Neuroscience, Liaoning Province, Dalian, PR China

^c State Key Laboratory of Brain and Cognitive Science, CAS Center for Excellence in Brain Science and Intelligence Technology, Institute of Psychology, Chinese Academy of Sciences, Beijing, PR China

^d Department of Psychology, University of Chinese Academy of Sciences, Beijing, PR China

^e Chinese Institute for Brain Research, Beijing, PR China

^f Institute of Artificial Intelligence, Hefei Comprehensive National Science Center, Hefei, PR China

ARTICLE INFO

Article history:

Received 9 June 2021

Reviewed 6 July 2021

Revised 30 August 2021

Accepted 30 November 2021

Action editor Clare Press

Published online 30 December 2021

Keywords:

Ebbinghaus illusion

Object manipulability

fMRI

Dynamic causal modeling

ABSTRACT

Action and perception interact reciprocally in our daily life. Previous studies have found that object manipulability can affect visual perceptual processing. Here we probed the neural mechanisms underlying the manipulability-related modulation effect using the well-known Ebbinghaus illusion with the central circle replaced by a high (i.e., a basketball) or a low (i.e., a watermelon) manipulable object. Participants ($N = 30$) were required to adjust the size of a comparison circle to match that of the central object in the Ebbinghaus configuration. The results showed that the perceived illusion magnitude for the basketball target was significantly reduced than that for the watermelon target, and the manipulability-related modulation effect was manifested in self-connections in the left primary visual cortex and the left superior parietal lobule (SPL), as well as reciprocal connections between the left lateral occipital cortex (LOC) and SPL. Notably, the disparity of the illusion magnitude between the watermelon and the basketball target was positively correlated with the extrinsic connectivity from the left LOC to SPL. The findings suggest that object manipulability can modulate the Ebbinghaus illusion, likely through accentuating the high-manipulability object along the visual processing streams. Moreover, they provide clear evidence that manipulability-related modulation of visual perception relies on the functional interactions between the ventral and dorsal visual pathways.

© 2021 Elsevier Ltd. All rights reserved.

* Corresponding author. Research Center of Brain and Cognitive Neuroscience, Liaoning Normal University, Dalian, PR China.

** Corresponding author. State Key Laboratory of Brain and Cognitive Science, CAS Center for Excellence in Brain Science and Intelligence Technology, Institute of Psychology, Chinese Academy of Sciences, Beijing, PR China.

E-mail addresses: lihongchen@lnnu.edu.cn (L. Chen), yijiang@psych.ac.cn (Y. Jiang).

<https://doi.org/10.1016/j.cortex.2021.11.019>

0010-9452/© 2021 Elsevier Ltd. All rights reserved.

1. Introduction

An object's action properties can affect both our cognitive processes and behavioral responses. For instance, the mere observation of pictures representing everyday manipulable objects results in facilitated cross-modal integration (Van Elk & Blanke, 2011). A manipulable object with similar action properties to a prime is recognized more accurately than those with dissimilar action properties (Helbig, Graf, & Kiefer, 2006; Helbig, Steinwender, Graf, & Kiefer, 2010; Kiefer, Sim, Helbig, & Graf, 2011). Pairs of action-related objects (i.e., a corkscrew and a bottle) are identified more accurately when they are positioned for action and oriented for use by the viewer's dominant hand (Roberts & Humphreys, 2011). In a visual search task, search performance is faster when the images depict action-related objects compared to non-action-related objects (Gomez & Snow, 2017). The above findings indicate that object manipulability can facilitate cognitive processes as revealed by more accurate and faster responses.

However, the neural mechanisms underlying manipulability-related facilitation of cognitive processes are largely unexplored. Here we probed this issue by using the Ebbinghaus illusion with the central circle replaced by a high (i.e., a basketball) or a low (i.e., a watermelon) manipulable object. In the Ebbinghaus illusion, the central object looks larger when surrounded by several small circles than when surrounded by several large ones. Previous studies have found that action-related features of an object are automatically processed, and the mere presentation of a manipulable object automatically potentiates object use information (Creem-Regehr & Lee, 2005; di Pellegrino, Rafal, & Tipper, 2005; Grezes, Tucker, Armony, Ellis, & Passingham, 2003; Tucker & Ellis, 1998). Manipulable objects elicit activation in both the dorsal stream consisting of the premotor, the inferior parietal, and the superior parietal cortices (Grezes et al., 2003; Tettamanti, Conca, Falini, & Perani, 2017), and the ventral stream including the lateral occipital cortex (LOC) and the fusiform gyrus (Kassuba et al., 2011; Roberts & Humphreys, 2010).

Converging evidence has found that human posterior parietal cortex and primary visual cortex (V1) are involved in visual size perception. For example, human posterior parietal cortex demonstrates object size-tuned responses in a topographic manner (Harvey, Fracasso, Petridou, & Dumoulin, 2015), and is also involved in the processing of object length (Borghesani et al., 2019). Interindividual variability of GABA level in the posterior parietal lobe significantly correlates with the magnitude of the Ebbinghaus illusion (Song, Sandberg, Andersen, Blicher, & Rees, 2017). Moreover, the superior parietal cortex is found to be associated with the processing of the Müller-Lyer illusion (Plewan, Weidner, Eickhoff, & Fink, 2012). In addition, visual size illusions have been found to be correlated with the functional and structural features of V1 (Chen et al., 2021; Fang, Boyaci, Kersten, & Murray, 2008; Murray, Boyaci, & Kersten, 2006; Pooremaeili, Arrighi, Biagi, & Morrone, 2013; Schwarzkopf, Song, & Rees, 2011; Wang, Chen, & Jiang, 2021).

Therefore, we expected that altered effective connectivity among cortical regions involved in the processing of object

manipulability and object size would be observed under the manipulability-related modulation of the Ebbinghaus illusion. It has been proposed that visual attribute (such as action-related features) determines whether information is processed in the ventral or dorsal pathway instead of whether the information is used for perception or action (de la Malla, Brenner, de Haan, & Smeets, 2019; Smeets & Brenner, 2019; Smeets, Kleijn, van der Meijden, & Brenner, 2020), and size illusions can be processed along both the ventral and the dorsal pathways, depending on which spatial attributes are used (Smeets, Brenner, de Grave, & Cuijpers, 2002). Thus, the modulation effect could affect the bidirectional connections between the ventral and the dorsal pathways, such as those between LOC and the superior parietal cortex (Plewan et al., 2012).

2. Materials and methods

2.1. Participants

Thirty participants (10 male, mean age = 21.5 ± 2.0 years) took part in the study. They were right-handed, reported normal or corrected-to-normal vision, and had no known neurological or visual disorders. They were naive to the purpose of the study, and gave written, informed consent. Sample size was determined based on our previous studies of the Ebbinghaus illusion (Chen, Qiao, Wang, & Jiang, 2018; Chen, Wu, Qiao, & Liu, 2020; Wang et al., 2021). The study was approved by the institutional review board of Liaoning Normal University and conducted in accordance with the tenets of the Declaration of Helsinki.

2.2. Stimuli and procedure

We selected a basketball as a high manipulable object (Tettamanti et al., 2017) and a watermelon as a low manipulable object. The difference of object manipulability between the basketball and watermelon target was confirmed by an online rating study. In particular, 20 participants were required to view and rate the manipulability of the basketball and the watermelon target on a 7-point Likert scale (1 = "low", 7 = "high") according to how easy it is to grasp and use the object with one hand (Salmon, McMullen, & Filliter, 2010). The results suggested that the basketball target was rated as more manipulable than the watermelon target ($t(19) = 7.26, p < .001, d = 1.62$). Low-level visual features such as physical size and mean luminance were adjusted and matched between these two objects.

Stimuli were generated using Matlab (Mathworks, Natick, MA) together with the Psychophysics Toolbox (Brainard, 1997; Pelli, 1997). In the illusion condition, the greyscale image of the watermelon or the basketball (.6°) target surrounded by four grey large (.9°) or small (.3°) inducers was presented for 400 msec, followed by a comparison circle presented in the lower field of the screen for 5500 msec (Fig. 1A and C). There was no spatial and temporal overlap between the illusory configuration and the comparison circle. The initial diameter of the comparison circle was randomly chosen from .46° to .66° for each trial. In the control condition (Fig. 1B), there was a

temporal gap of 1000 msec between the presentations of the inducers and the target in order to reduce or eliminate the illusion effect, according to previous studies (Cooper & Weintraub, 1970; Jaeger & Pollack, 1977). In both conditions, participants were required to adjust the size of the comparison circle to match that of the central target by repeatedly pressing up and down response keys to respectively increase and decrease the size of the comparison circle within 5500 msec.

2.3. MRI data acquisition

In the scanner, the stimuli were back-projected via a video projector (60 Hz, 1280 × 1024) onto a translucent screen placed inside the scanner bore. Participants viewed the stimuli through a mirror located above their eyes. Functional MRI data were collected using a 3T scanner (MR-750, GE medical systems, Milwaukee, WI) with an 8-channel phase-array coil. BOLD signals were measured with a gradient echo-planar imaging sequence (echo time = 29 msec, repetition time = 2000 msec, field of view = 192 mm, matrix = 64 × 64, flip angle = 90°, number of slices = 43, spatial resolution = 3 × 3 × 3 mm³). A high-resolution 3D structural dataset (echo time = 2.9 msec, repetition time = 6.7 msec, field of view = 256 mm, matrix = 256 × 256, flip angle = 12°, spatial resolution = 1 × 1 × 1 mm³) was collected for each participant. To minimize head movements, straps and foam pads were used to fix the head comfortably during scanning. The first three scans were discarded to allow for magnetic field stabilization.

2.4. Designs

There were 8 experimental conditions: target type (watermelon and basketball) × size of inducers (large and small) × presentation sequence (simultaneous and sequential). We used an event-related design and added 50% null trials

among 8 functional runs, each with a duration of 256 sec. Each run consisted of sixteen 8-sec stimuli presentation with random distributed 2-sec blank intervals whose overall time was 128 sec. The best stimuli sequence and onset time of the blank intervals were calculated by AFNI's RSFgen program (<http://afni.nimh.nih.gov>), to maximize hemodynamic signal sensitivity. We considered in our analyses only the brain responses evoked during the first 2-sec of each trial including the presentation of the fixation and components of the illusory configuration (i.e., the surrounding inducers and the central target), in which no active comparison task was performed, to ensure that neural responses in the processing of the illusory configuration would not be related to the comparison process itself (Borghesani et al., 2019).

A separate functional localizer run was conducted, which composed of eight 16-sec blocks with alternating blocks between intact objects and scrambled images that were presented centrally (2.6° × 3.4°). Participants were asked to perform 1-back repetition detection task whenever two successive images were identical. For each participant, LOC was defined by the contrast between intact and scrambled images with a t-map threshold of $p < .05$, FWE corrected.

2.5. MRI data processing and analysis

Image time-series were preprocessed and analyzed using SPM12 (r7487). Images were slice timing corrected, spatially normalized into a standard stereotactic space (Montreal Institute on Neurology, MNI template) and smoothed using an isotropic 6-mm Gaussian kernel. Low frequency noise was removed through the use of a high-pass filter (cutoff 1/128 Hz), and time-series were corrected for serial autocorrelations using a first-order autoregressive [AR(1)] model.

Regions of interest (ROIs) included bilateral V1, LOC and the superior parietal lobule (SPL). MNI coordinates of V1 (left: -14, -100, 0; right: 14, -96, -2) were literature-defined from

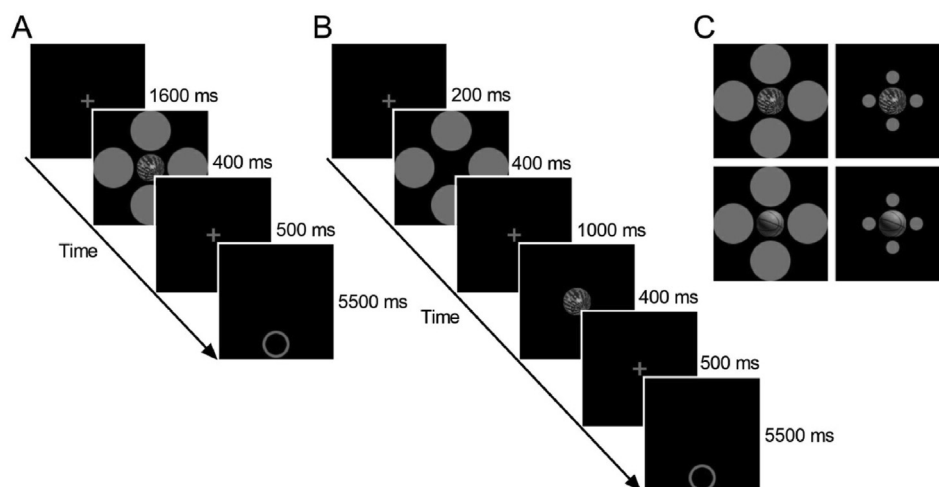


Fig. 1 – Schematic representation of experimental procedure and stimuli. (A) In the illusion condition, a watermelon or a basketball target surrounded by four large or small inducers was presented for 400 msec followed by a comparison circle. Participants were required to adjust the size of the comparison circle to match that of the watermelon or basketball target within 5500 msec. (B) In the control condition, the surrounding inducers and the central target were presented in succession with a temporal gap of 1000 msec, followed by a comparison circle. (C) Illustration of stimuli used in the illusion condition.

previously published fMRI research on visual size illusion (Weidner et al., 2014), and coordinates of LOC (left: $-39, -79, 14$; right: $48, -73, 11$; see Fig. 2) were based on the contrast between intact and scrambled objects ($p < .05$, FWE corrected). Coordinates of SPL (left: $-21, -52, 59$; right: $18, -58, 56$) were obtained from the contrast of the illusion condition in comparison to the control condition ($p < .001$, uncorrected). We summarized the BOLD signal in each participant using the first eigenvariate (principal component) of voxels within a sphere of 8 mm radius (Lumaca, Dietz, Hansen, Quiroga-Martinez, & Vuust, 2021) centered on each participant's local maximum within bilateral V1, LOC and SPL.

Effective connectivities among V1, LOC and SPL were analyzed separately in the left and right hemispheres using dynamic causal modeling (DCM) in SPM12. DCM models the hierarchical organization of the brain using self-connections within a region, as well as forward and backward connections between regions (Lumaca et al., 2021). The model space consisted of a full model (Model A) and a reduced model (Model B), both of which had the same basic architecture and differed only with respect to which connections (i.e., the bidirectional connections between V1 and SPL) were allowed to vary to explain the manipulability-related modulation of the illusion effect (Fig. 8A). In Model A, all the eight experimental conditions served as the modulatory effect on all the connections among the three ROIs. It has been found that the strength of the Müller-Lyer illusion modulates the bidirectional connections between LOC and the superior parietal cortex rather than those between V1 and the superior parietal cortex (Plewan et al., 2012). Therefore, Model B featured a connectivity architecture that was equivalent to Model A with the exclusion of bidirectional connections between V1 and SPL. We used Bayesian Model Reduction (BMR) to evaluate the evidence for these two models, and reported the posterior estimates under each model. All the eight experimental conditions were used as driving inputs into V1, which is lowest in hierarchy (Van de Steen, Krebs, Colenbier, Almgren, & Marinazzo, 2020).

3. Results

3.1. Behavioral results

The illusion magnitude was measured as the difference of the perceived size of the central target surrounded by small

and large inducers relative to its physical size (%). In the illusion condition, the illusion magnitude compared with zero was significant for both the watermelon ($M = 13.9\%$, $t(29) = 10.66$, $p < .001$, $d = 1.95$) and the basketball ($M = 11.1\%$, $t(29) = 9.90$, $p < .001$, $d = 1.81$) targets, with the former being significantly larger than the latter ($t(29) = 4.78$, $p < .001$, $d = .87$; Fig. 3A). However, in the control condition, the illusion effect disappeared (watermelon: $M = -.3\%$, $t(29) = -.40$, $p = .695$, $d = .07$; basketball: $M = -.1\%$, $t(29) = -.19$, $p = .852$, $d = .03$; Fig. 3B). When the illusion effect in the control condition was subtracted from that in the illusion condition, similar patterns of results were observed. In particular, the illusion magnitude was significant for both the watermelon ($M = 14.2\%$, $t(29) = 9.80$, $p < .001$, $d = 1.79$) and the basketball ($M = 11.2\%$, $t(29) = 10.58$, $p < .001$, $d = 1.93$) targets, and the former was significantly larger than the latter ($t(29) = 2.90$, $p = .007$, $d = .53$).

3.2. Group level GLM

Brain regions that responded to the illusion condition in contrast to the control condition were shown in Fig. 4 ($p < .001$, uncorrected). As expected, this whole volume analysis revealed robust activations throughout the occipital cortex, as well as bilateral SPL (left: $-21, -52, 59$; right: $18, -58, 56$). It should be noted that the activations in bilateral SPL did not survive correction for multiple comparisons, but these two regions were still adopted for further DCM analysis because converging evidence has demonstrated their involvement in the processing of both visual size illusions and object manipulability. When the four illusory stimuli (a basketball or a watermelon target surrounded by large or small inducers) was examined separately, robust activations throughout the occipital cortex were still observed in contrast to their corresponding control conditions (Table 1, Figs. 5 and 6). Moreover, when a watermelon was surrounded by small inducers, activations were also observed in bilateral inferior and superior parietal lobules, as well as bilateral inferior frontal gyri and insula. However, in the control condition (Fig. 7), no significant activation was observed for the watermelon target preceded by small inducers in contrast to large inducers ($p < .001$, uncorrected), and only frontal regions including inferior and middle frontal gyrus were activated by the basketball target condition ($p < .001$, uncorrected).

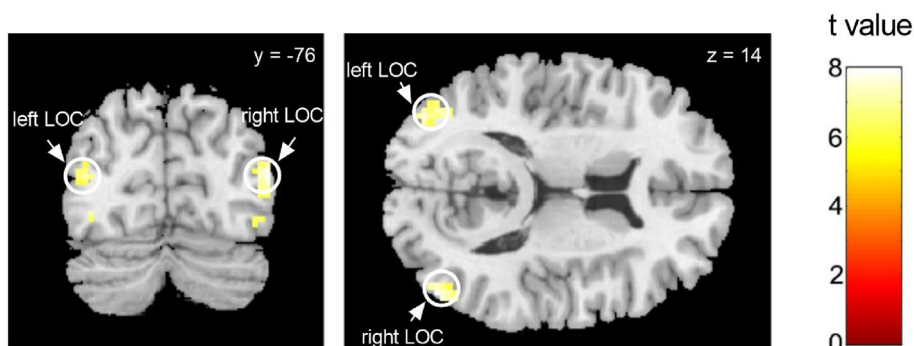


Fig. 2 – Group analysis of the LOC localizer (objects minus scrambled objects) with a threshold of $p < .05$, FWE corrected.

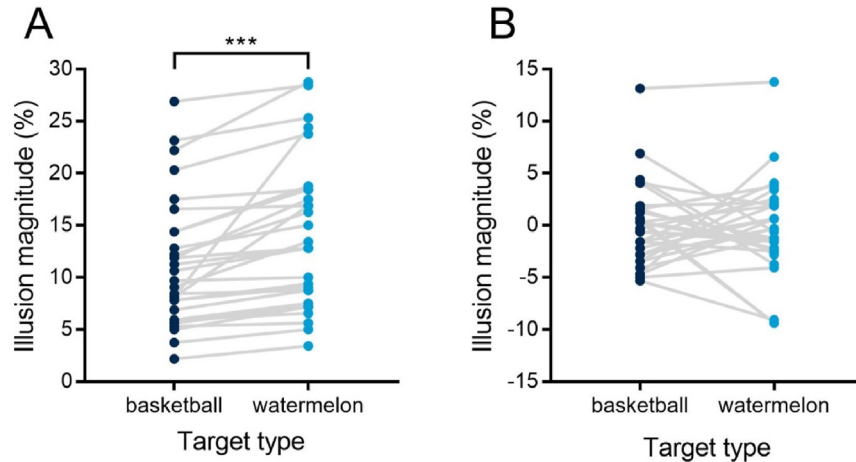


Fig. 3 – Results of behavioral measurements. Illusion magnitudes in (A) the illusion condition and (B) the control condition. Asterisks (*) indicate a significance level of $*p < .001$.**

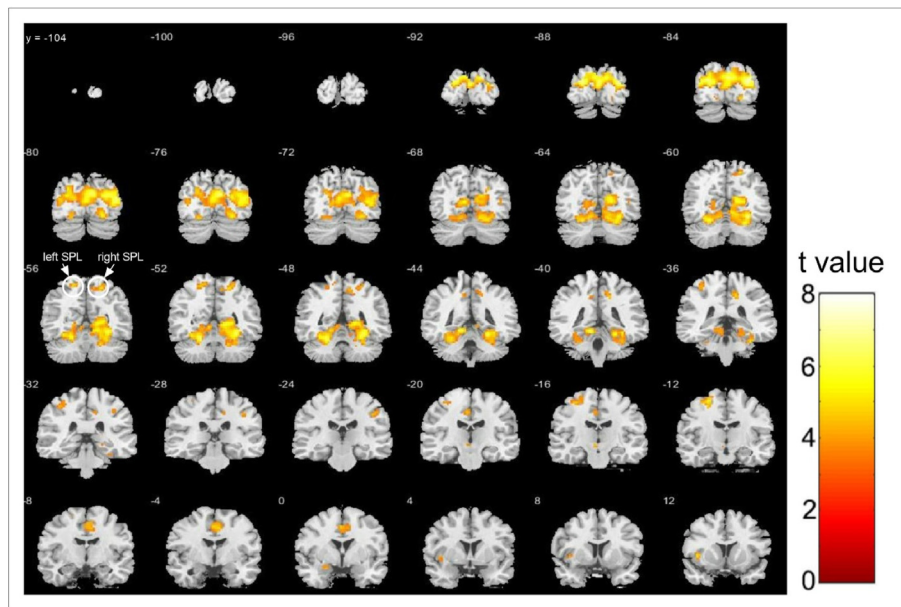


Fig. 4 – Cortical areas responding to the illusion condition in contrast to the control condition ($p < .001$, uncorrected). White circles indicate the locations of the left and right superior parietal lobule (SPL).

3.3. Connectivity results

In the left hemisphere, the evidence for model B (posterior probability = .57) was higher than that for model A (posterior probability = .43; see Fig. 8B). For the winning model (i.e., model B; Fig. 8C), the results of effective connectivity showed that the manipulability-related modulation effect was manifested by significantly increased self-connection in V1 (paired t-tests; $M = .05$, $t(29) = 2.62$, $p = .014$, $d = .48$) and significantly decreased self-connection in SPL ($M = -.10$, $t(29) = -2.79$, $p = .009$, $d = .51$), as well as significantly strengthened reciprocal connections between LOC and SPL (from LOC to SPL: $M = .19$, $t(29) = 2.90$, $p = .007$, $d = .53$; from SPL to LOC: $M = .05$, $t(29) = 2.56$, $p = .016$, $d = .47$). However, significantly altered effective connectivity was not observed in the control condition ($ps > .13$). When directly comparing the illusion condition with the control

condition (paired t-tests), similar patterns of results were observed. Specifically, the manipulability-related modulation effect was demonstrated by significant self-connections in V1 ($M = .07$, $t(29) = 2.73$, $p = .011$, $d = .50$) and SPL ($M = -.13$, $t(29) = -2.82$, $p = .009$, $d = .52$), as well as significant forward connection from LOC to SPL ($M = .25$, $t(29) = 2.74$, $p = .010$, $d = .50$). Moreover, behavioral performance (i.e., the disparity of illusion magnitudes between the watermelon and the basketball target) was positively correlated with the extrinsic connectivity from LOC to SPL that was associated with manipulability-related modulation effect ($r(30) = .38$, $p = .040$, 95% confidence interval = [.02, .65]; see Fig. 8D).

In the right hemisphere, the evidence for model B (posterior probability = .37) was lower than that for model A (posterior probability = .63). The results of effective connectivity for the winning model (i.e., model A) showed that significant

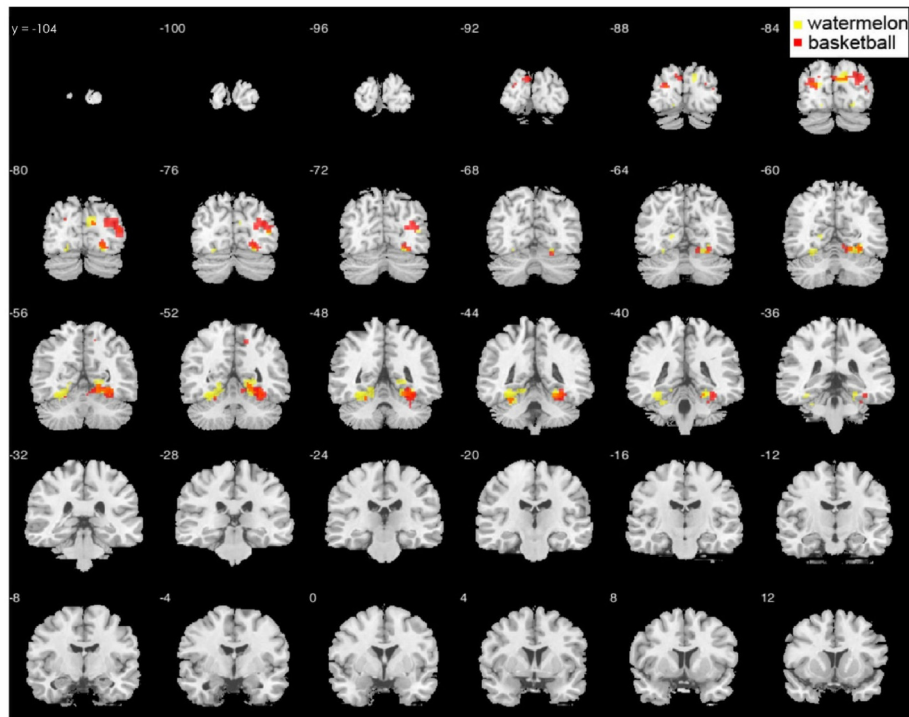


Fig. 5 – Cortical areas responding to the target (watermelon: yellow; basketball: red) surrounded by large inducers in contrast to the corresponding control condition ($p < .001$, uncorrected).

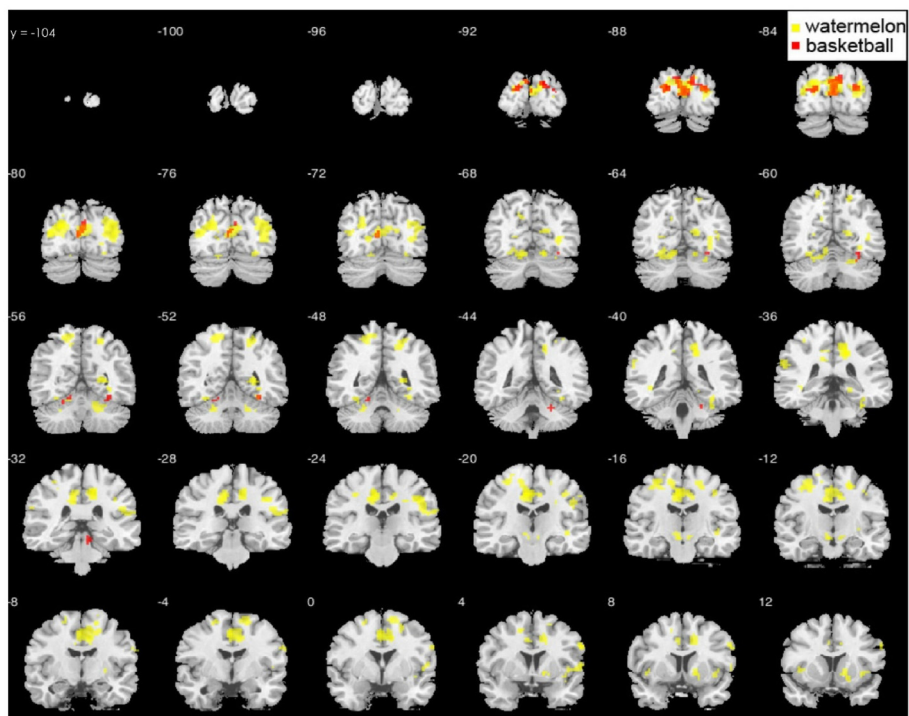


Fig. 6 – Cortical areas responding to the target (watermelon: yellow; basketball: red) surrounded by small inducers in contrast to the corresponding control condition ($p < .001$, uncorrected).

effect of manipulability-related modulation on the Ebbinghaus illusion was not observed in any of self-connections and extrinsic connections under both the illusion and the control

condition ($ps > .15$), and similar patterns of results were observed when directly comparing the illusion condition with the control condition ($ps > .23$).

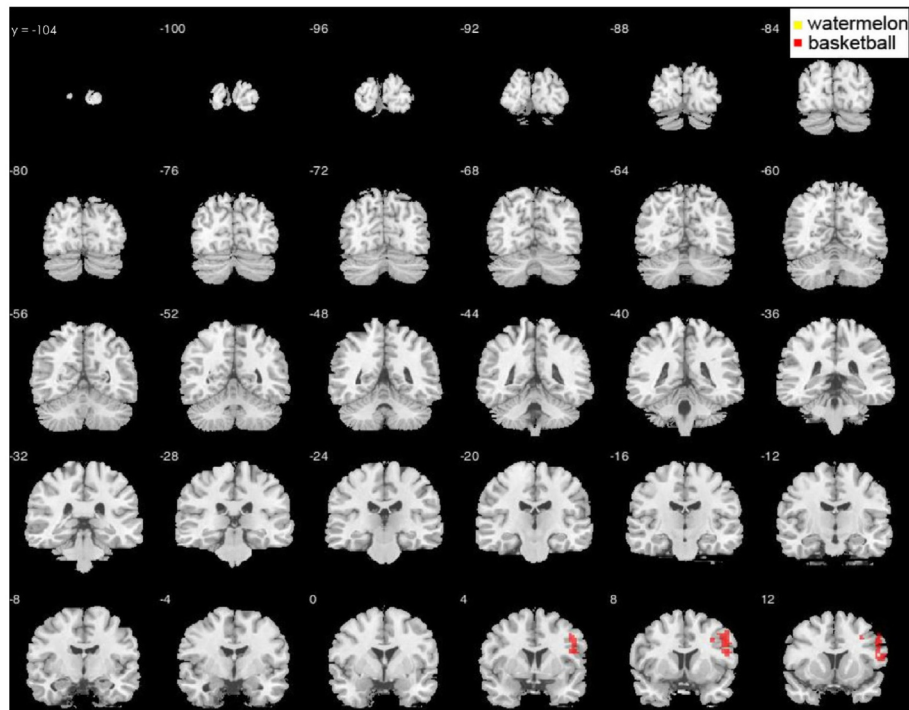


Fig. 7 – Cortical activations in response to the target (watermelon: yellow; basketball: red) preceded by small inducers relative to large inducers in the control condition ($p < .001$, uncorrected).

4. Discussion

The current study investigated the neural mechanisms underlying the manipulability-related modulation of context-dependent visual size perception by focusing on effective connectivities among cortical regions that are associated with the processing of object manipulability and object size (i.e., bilateral V1, LOC and SPL). Behavioral results showed that the illusion magnitude for a basketball target was significantly smaller than that for a watermelon target. DCM results revealed that manipulability-related modulation effect was observed in self-connections in V1 and SPL, as well as reciprocal connections between LOC and SPL in the left instead of the right hemisphere. Notably, the disparity of the illusion magnitudes between the watermelon and the basketball targets was positively correlated with the extrinsic connectivity from the left LOC to SPL.

Previous studies have shown that object manipulability facilitates the allocation of spatial attention towards the location of manipulable objects (Van Elk & Blanke, 2011). High-manipulability objects likely receive more automatic prioritization of attentional resources compared to low-manipulability objects. Specifically, in contrast to low-manipulability stimuli, high-manipulability stimuli elicit larger P1 and P300 amplitudes, the latter of which reflects both bottom-up and top-down attention processes (Handy & Tipper, 2007; Madan, Chen, & Singhal, 2016). Likewise, the amplitude of P1 elicited by the target presented in the right visual field was larger when it was superimposed on a tool object than on a non-tool object (Handy, Grafton, Shroff, Ketay, & Gazzaniga, 2003). In an attentional blink paradigm,

providing an action relationship between T1 and T2 leads to enhanced attentional selection and consolidation of T2, as demonstrated by a diminished blink and an enhanced P3 amplitude (Adamo & Ferber, 2009). Moreover, patients suffered from visual extinction after right-parietal injury show reduced extinction when cups have handles affording a left-hand grasp, even though no hand response is required (di Pellegrino et al., 2005), and they are able to better identify two concurrently presented objects that appear to be interacting than pairs of objects placed in incorrect positions for their combined use (Riddoch, Humphreys, Edwards, Baker, & Willson, 2003). Therefore, in the current study, the relatively high-manipulability basketball might attract more attentional resources than the low-manipulability watermelon, thus less attention is allocated to the inducers surrounding the basketball target and further leads to the reduced illusion magnitude.

Converging evidence has found the involvement of LOC in the processing of object manipulability (Ishibashi, Pobric, Saito, & Lambon Ralph, 2016). In particular, relative to non-object control stimuli, manipulable objects lead to an enhanced activation in bilateral LOC and the fusiform gyrus (Kassuba et al., 2011). Object-related LOC is activated by both visual and tactile recognition of manipulable objects relative to scrambled versions of the same objects or textures (Amedi, Jacobson, Hendler, Malach, & Zohary, 2002; Amedi, Malach, Hendler, Peled, & Zohary, 2001). Furthermore, correct tool manipulation produced significant activations at both bilateral parietofrontal areas and bilateral occipitotemporal cortex including the middle occipital gyrus in comparison to incorrect tool manipulation (Mizelle, Kelly, & Wheaton, 2013). During real action planning and execution phases, both the

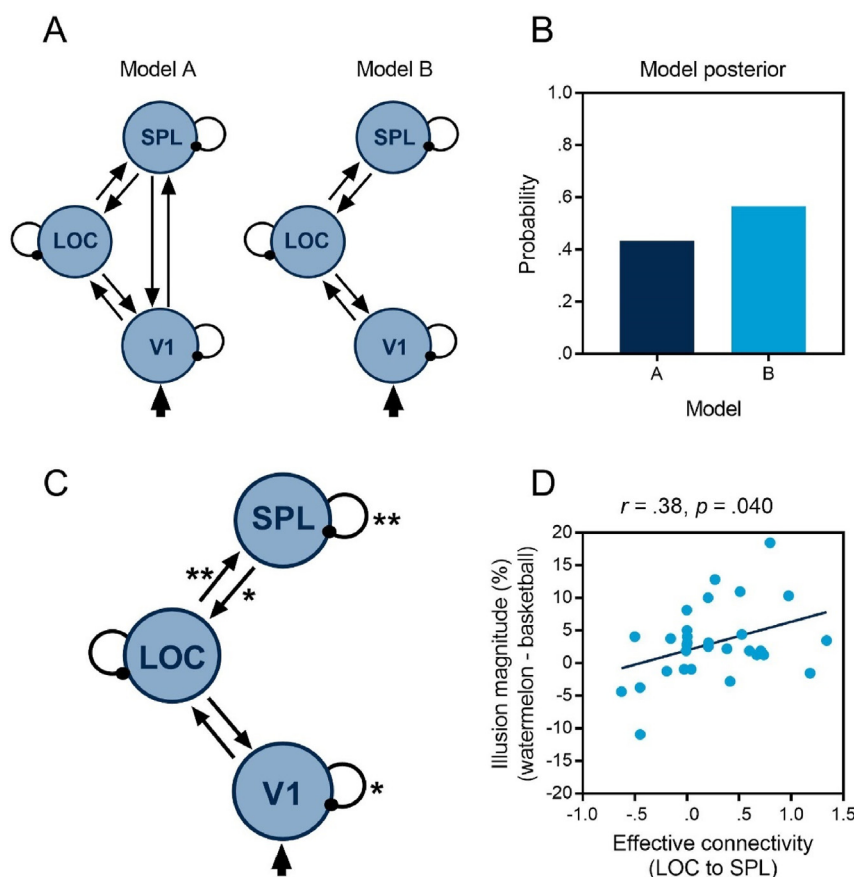


Fig. 8 – Model space and DCM Results. (A) Model space (black lines indicate latent connectivity, thick arrow indicates driving input) and (B) model evidence estimated by Bayesian Model Reduction. (C) Schematic representation of the manipulability-related modulation effect on the Ebbinghaus illusion (watermelon – basketball) for Model B in the left hemisphere. Asterisks indicate significant modulation effect. (D) Correlation of behavioral performance (i.e., the disparity of the illusion magnitudes between the watermelon and the basketball target) with effective connectivity from the left LOC to SPL that corresponds to the modulation effect. Asterisks (*) indicate a significance level of $* p < .05$ and $p < .01$.**

left LOC and SPL show greater activations to tools than neutral objects (i.e., bars) (Brandi, Wohlschläger, Sorg, & Hermsdörfer, 2014). In line with and extending the above evidence, the current study showed positive effective connectivity between the left LOC and SPL under manipulability-related modulation of visual size perception. These positive values indicate that an increase of neural activity in the source region results in an increase of neural activity in the target region.

Moreover, the self-connection in the left SPL was negative when comparing the illusion effect of the watermelon target with that of the basketball target. The more positive the self-connection parameter for the basketball target condition, the more inhibited the region (i.e., the left SPL), and the less this region responded to its inputs (Zeidman et al., 2019). Therefore, the left SPL response to the inducers surrounding the basketball target was more suppressive than to the inducers surrounding the watermelon target. The findings together with previous studies suggest that object manipulability can be processed in the ventral LOC, and further projects to the dorsal SPL to modulate cognitive processes. As a previous study has shown a positive correlation between the parietal GABA level and the Ebbinghaus illusion magnitude (Song et al., 2017), thus the forward projection from LOC might

decrease the GABA level in the SPL, and further leads to the reduced illusion effect. Notably, we observed a left hemispheric asymmetry of the network involved in the manipulability-related modulation effect, possibly due to the left lateralized processing bias for the Ebbinghaus illusion (Chen et al., 2021; Schwarzkopf et al., 2011) and/or for manipulable objects (Goldenberg & Spatt, 2009; Styrkowiec, Nowik, & Króliczak, 2019).

Recent work has shown that there are significant interactions between the ventral and the dorsal streams, as demonstrated by some overlap in their functions and reciprocal connections between the two streams (Almeida, Fintzi, & Mahon, 2013). For instance, increased functional connectivity between the frontoparietal network and the ventral occipitotemporal cortex is observed when participants viewing tools in contrast to animals (Almeida et al., 2013), watching videos of manipulation actions such as folding (Yang, He, Han, & Bi, 2020), generating tool pantomimes (Garcea, Chen, Vargas, Narayan, & Mahon, 2018), as well as performing motor-based tasks (Garcea & Buxbaum, 2019; Hutchison & Gallivan, 2018). Kristensen, Garcea, Mahon, and Almeida (2016) used images of tools and animals and presented them at low (5 Hz) and high (15 Hz) temporal

Table 1 – Peak coordinates of the whole brain analysis with the contrast between the illusion condition and the control condition ($p < .001$, uncorrected; BL = a basketball target surrounded by large inducers, BS = a basketball target surrounded by small inducers; WL = a watermelon target surrounded by large inducers, WS = a watermelon target surrounded by small inducers; Hemi. = Hemisphere; Clust. = Cluster size).

Condition	Region	Hemi.	Clust.	t	Peak coordinates MNI		
					x	y	z
BL	fusiform gyrus	R	211	5.99	30	−49	−19
	fusiform gyrus	L	15	4.04	−27	−43	−22
	lingual gyrus	R	38	4.71	21	−76	−7
	middle occipital gyrus	R	188	5.24	42	−82	11
	middle occipital gyrus	L	28	4.22	−27	−88	17
BS	fusiform gyrus	R	29	4.57	30	−58	−13
	cuneus	R	168	5.27	12	−91	23
	middle occipital gyrus	L	31	4.76	−18	−91	17
WL	fusiform gyrus	L	201	5.70	−33	−46	−16
	fusiform gyrus	R	217	7.02	24	−43	−16
	lingual gyrus	L	13	3.88	−21	−79	−10
	middle occipital gyrus	L	17	3.97	−21	−85	17
	cuneus	R	67	5.07	9	−85	26
WS	fusiform gyrus	R	20	5.17	33	−37	−25
	fusiform gyrus	L	114	4.88	−15	−67	−16
	midbrain	R	11	3.95	6	−16	−10
	midbrain	L	19	5.49	−6	−13	−13
	insula	R	195	4.88	33	17	−4
	middle occipital gyrus	R	299	5.18	36	−79	8
	insula	L	63	4.93	−24	29	−1
	cuneus	L	590	6.12	−27	−79	20
	inferior frontal gyrus	R	14	3.94	51	41	5
	inferior frontal gyrus	L	22	4.28	−45	29	11
	limbic lobe	L	605	6.19	−9	−19	44
	inferior parietal lobule	R	140	5.15	42	−25	35
	inferior parietal lobule	L	27	4.09	−60	−37	26
	inferior frontal gyrus	R	33	6.01	57	5	32
	middle frontal gyrus	L	43	4.96	−33	35	32
	superior parietal lobule	R	184	6.19	15	−37	41
	precentral gyrus	L	101	4.91	−30	−16	59
	superior parietal lobule	L	78	4.67	−21	−52	59
	postcentral gyrus	L	12	4.00	−36	−34	59
	medial frontal gyrus	L	11	4.42	−15	5	53

frequencies to respectively bias processing toward the parvocellular and the magnocellular pathways, and found that tool preferences under low temporal frequency were restricted to the inferior parietal lobule, suggesting that the inferior parietal lobule receives inputs from the ventral visual pathway. Further, tool preferences in left ventral temporal cortex are inversely related to the likelihood of a lesion to left anterior intraparietal sulcus, suggesting that part of the ventral visual hierarchy incorporates inputs from the dorsal visual pathway (Garcea et al., 2019). Taken together, the above evidence in favor of functional interactions of the two visual pathways has used experimental tasks that are directly related with tools, such as tool viewing, tool manipulation, and tool pantomime.

Sim, Helbig, Graf, and Kiefer (2015) found increased functional connectivity from the left superior parietal cortex to the left anterior temporal area for the action priming effect on the visual recognition of manipulable objects. In the current study, we adopted a non-tool manipulable object and a size matching task, and still observed significant functional connectivity between the ventral and the dorsal pathways during manipulability-related modulation of visual perception.

Moreover, this functional connectivity was significantly correlated with behavioral performance. The findings support the idea of automatic processing of object manipulability, and reveal that manipulability-related modulation of visual size perception relies on the functional interactions of the two visual pathways.

There are some limitations to be considered in the current study. We analyzed the brain responses evoked by the first 2-sec of each trial for both the illusion and the control condition. During this period, the surrounding inducers and the central target were presented simultaneously or sequentially with a gap of 1000 msec for the illusion and the control condition, respectively. Though we kept the physical stimuli as identical as possible for these two conditions, some cognitive processes, such as memory, might still be different. Future study could adopt another control condition to avoid the potential confounding influence when investigating the processing of the Ebbinghaus illusion.

In summary, the current study shows that object manipulability can reduce the size illusion magnitude, which might be caused by the automatic attentional attraction to the manipulable object and the resulting reduced attentional

allocation to the surrounding inducers. Moreover, such manipulability-related modulation of the visual size illusion is associated with reciprocal connectivity between LOC and SPL in the left hemisphere, in favor of the functional interactions of the ventral and the dorsal visual pathways.

Credit author statement

Lihong Chen: Conceptualization, Formal analysis, Writing – original draft, Writing – review & editing. **Shengnan Zhu:** Data acquisition. **Bengang Feng:** Data acquisition. **Xue Zhang:** Formal analysis. **Yi Jiang:** Conceptualization, Supervision, Writing – original draft, Writing – review & editing.

Open practices

No part of the study procedures and study analyses was pre-registered prior to the research being conducted. We applied known analytic methods for data analysis with the details provided in the study; there were no custom-written analysis code. We reported how we determined our sample size, all data exclusions (if any), all inclusion/exclusion criteria, whether inclusion/exclusion criteria were established prior to data analysis, all manipulations, and all measures in the study.

The study in this article earned an Open Materials badge for transparent practices. The conditions of our ethics approval do not permit public archiving of individual anonymized study data. Readers seeking access to the data should contact to the corresponding authors. Access to anonymized data will be granted to named individuals. There are no further conditions. Stimuli and experiment code can be found here: <https://osf.io/syxvn/>.

Declaration of competing interest

None declared.

Acknowledgments

This work was supported by grants from the Ministry of Science and Technology of the People's Republic of China (2021ZD0203801), the National Natural Science Foundation of China (No. 32171047, No. 31830037, No. 31700946, No. 31525011), the Strategic Priority Research Program and the Key Research Program of Frontier Sciences of the Chinese Academy of Sciences (No. XDB32010300, No. QYZDB-SSW-SMC030), the Fundamental Research Funds for the Central Universities, and the Scientific Study Project for Department of Education of Liaoning Province (No. LJKZ0969).

REFERENCES

Adamo, M., & Ferber, S. (2009). A picture says more than a thousand words: Behavioural and ERP evidence for attentional

- enhancements due to action affordances. *Neuropsychologia*, 47(6), 1600–1608. <https://doi.org/10.1016/j.neuropsychologia.2008.07.009>
- Almeida, J., Fintzi, A. R., & Mahon, B. Z. (2013). Tool manipulation knowledge is retrieved by way of the ventral visual object processing pathway. *Cortex*, 49(9), 2334–2344. <https://doi.org/10.1016/j.cortex.2013.05.004>
- Amedi, A., Jacobson, G., Hendler, T., Malach, R., & Zohary, E. (2002). Convergence of visual and tactile shape processing in the human lateral occipital complex. *Cerebral Cortex*, 12(11), 1202–1212. <https://doi.org/10.1093/cercor/12.11.1202>
- Amedi, A., Malach, R., Hendler, T., Peled, S., & Zohary, E. (2001). Visuo-haptic object-related activation in the ventral visual pathway. *Nature Neuroscience*, 4(3), 324–330. <https://doi.org/10.1038/85201>
- Borghesani, V., de Hevia, M. D., Viarouge, A., Pinheiro-Chagas, P., Eger, E., & Piazza, M. (2019). Processing number and length in the parietal cortex: Sharing resources, not a common code. *Cortex*, 114, 17–27. <https://doi.org/10.1016/j.cortex.2018.07.017>
- Brainard, D. H. (1997). The psychophysics toolbox. *Spatial Vision*, 10, 433–436. <https://doi.org/10.1163/156856897X00357>
- Brandi, M.-L., Wohlschläger, A., Sorg, C., & Hermsdörfer, J. (2014). The neural correlates of planning and executing actual tool use. *The Journal of Neuroscience*, 34(39), 13183–13194. <https://doi.org/10.1523/jneurosci.0597-14.2014>
- Chen, L., Qiao, C., Wang, Y., & Jiang, Y. (2018). Subconscious processing reveals dissociable contextual modulations of visual size perception. *Cognition*, 180, 259–267. <https://doi.org/10.1016/j.cognition.2018.07.014>
- Chen, L., Wu, B., Qiao, C., & Liu, D.-Q. (2020). Resting EEG in alpha band predicts individual differences in visual size perception. *Brain and Cognition*, 145, 105625. <https://doi.org/10.1016/j.bandc.2020.105625>
- Chen, L., Xu, Q., Shen, L., Yuan, T., Wang, Y., Zhou, W., et al. (2021). Distinct contributions of genes and environment to visual size illusion and the underlying neural mechanism. *Cerebral Cortex*. <https://doi.org/10.1093/cercor/bhab262>
- Cooper, L. A., & Weintraub, D. J. (1970). Delboeuf-type circle illusions: Interactions among luminance, temporal characteristics, and inducing-figure variations. *Journal of Experimental Psychology*, 85(1), 75–82. <https://doi.org/10.1037/h0029503>
- Creem-Regehr, S. H., & Lee, J. N. (2005). Neural representations of graspable objects: Are tools special? *Cognitive Brain Research*, 22(3), 457–469. <https://doi.org/10.1016/j.cogbrainres.2004.10.006>
- de la Malla, C., Brenner, E., de Haan, E. H. F., & Smeets, J. B. J. (2019). A visual illusion that influences perception and action through the dorsal pathway. *Communications Biology*, 2(1), 38. <https://doi.org/10.1038/s42003-019-0293-x>
- di Pellegrino, G., Rafal, R., & Tipper, S. P. (2005). Implicitly evoked actions modulate visual selection: Evidence from parietal extinction. *Current Biology*, 15(16), 1469–1472. <https://doi.org/10.1016/j.cub.2005.06.068>
- Fang, F., Boyaci, H., Kersten, D., & Murray, S. O. (2008). Attention-dependent representation of a size illusion in human V1. *Current Biology*, 18(21), 1707–1712. <https://doi.org/10.1016/j.cub.2008.09.025>
- Garcea, F. E., Almeida, J., Sims, M. H., Nunno, A., Meyers, S. P., Li, Y. M., ... Mahon, B. Z. (2019). Domain-specific diaschisis: Lesions to parietal action areas modulate neural responses to tools in the ventral stream. *Cerebral Cortex*, 29(7), 3168–3181. <https://doi.org/10.1093/cercor/bhy183>
- Garcea, F. E., & Buxbaum, L. J. (2019). Gesturing tool use and tool transport actions modulates inferior parietal functional connectivity with the dorsal and ventral object processing pathways. *Human Brain Mapping*, 40(10), 2867–2883. <https://doi.org/10.1002/hbm.24565>
- Garcea, F. E., Chen, Q. J., Vargas, R., Narayan, D. A., & Mahon, B. Z. (2018). Task- and domain-specific modulation of functional

- connectivity in the ventral and dorsal object-processing pathways. *Brain Structure & Function*, 223(6), 2589–2607. <https://doi.org/10.1007/s00429-018-1641-1>
- Goldenberg, G., & Spatt, J. (2009). The neural basis of tool use. *Brain*, 132(6), 1645–1655. <https://doi.org/10.1093/brain/awp080>
- Gomez, M. A., & Snow, J. C. (2017). Action properties of object images facilitate visual search. *Journal of Experimental Psychology: Human Perception and Performance*, 43(6), 1115–1124. <https://doi.org/10.1037/xhp0000390>
- Grezes, J., Tucker, M., Armony, J., Ellis, R., & Passingham, R. E. (2003). Objects automatically potentiate action: An fMRI study of implicit processing. *European Journal of Neuroscience*, 17(12), 2735–2740. <https://doi.org/10.1046/j.1460-9568.2003.02695.x>
- Handy, T. C., Grafton, S. T., Shroff, N. M., Ketay, S., & Gazzaniga, M. S. (2003). Graspable objects grab attention when the potential for action is recognized. *Nature Neuroscience*, 6(4), 421–427. <https://doi.org/10.1038/nn1031>
- Handy, T. C., & Tipper, C. M. (2007). Attentional orienting to graspable objects: What triggers the response? *Neuroreport*, 18(9), 941–944. <https://doi.org/10.1097/wnr.0b013e3281332674>
- Harvey, B. M., Fracasso, A., Petridou, N., & Dumoulin, S. O. (2015). Topographic representations of object size and relationships with numerosity reveal generalized quantity processing in human parietal cortex. *Proceedings of the National Academy of Sciences of the United States of America*, 112(44), 13525–13530. <https://doi.org/10.1073/pnas.1515414112>
- Helbig, H. B., Graf, M., & Kiefer, M. (2006). The role of action representations in visual object recognition. *Experimental Brain Research*, 174(2), 221–228. <https://doi.org/10.1007/s00221-006-0443-5>
- Helbig, H. B., Steinwender, J., Graf, M., & Kiefer, M. (2010). Action observation can prime visual object recognition. *Experimental Brain Research*, 200(3–4), 251–258. <https://doi.org/10.1007/s00221-009-1953-8>
- Hutchison, R. M., & Gallivan, J. P. (2018). Functional coupling between frontoparietal and occipitotemporal pathways during action and perception. *Cortex*, 98, 8–27. <https://doi.org/10.1016/j.cortex.2016.10.020>
- Ishibashi, R., Pobric, G., Saito, S., & Lambon Ralph, M. A. (2016). The neural network for tool-related cognition: An activation likelihood estimation meta-analysis of 70 neuroimaging contrasts. *Cognitive Neuropsychology*, 33(3–4), 241–256. <https://doi.org/10.1080/02643294.2016.1188798>
- Jaeger, T., & Pollack, R. H. (1977). Effect of contrast level and temporal order on the Ebbinghaus circles illusion. *Perception & Psychophysics*, 21(1), 83–87. <https://doi.org/10.3758/BF03199473>
- Kassuba, T., Klinge, C., Holig, C., Menz, M. M., Ptito, M., Roder, B., et al. (2011). The left fusiform gyrus hosts trisensory representations of manipulable objects. *Neuroimage*, 56(3), 1566–1577. <https://doi.org/10.1016/j.neuroimage.2011.02.032>
- Kiefer, M., Sim, E.-J., Helbig, H., & Graf, M. (2011). Tracking the time course of action priming on object recognition: Evidence for fast and slow influences of action on perception. *Journal of Cognitive Neuroscience*, 23(8), 1864–1874. <https://doi.org/10.1162/jocn.2010.21543>
- Kristensen, S., Garcea, F. E., Mahon, B. Z., & Almeida, J. (2016). Temporal frequency tuning reveals interactions between the dorsal and ventral visual streams. *Journal of Cognitive Neuroscience*, 28(9), 1295–1302. https://doi.org/10.1162/jocn_a_00969
- Lumaca, M., Dietz, M. J., Hansen, N. C., Quiroga-Martinez, D. R., & Vuust, P. (2021). Perceptual learning of tone patterns changes the effective connectivity between Heschl's gyrus and planum temporale. *Human Brain Mapping*, 42(4), 941–952. <https://doi.org/10.1002/hbm.25269>
- Madan, C. R., Chen, Y. Y., & Singhal, A. (2016). ERPs differentially reflect automatic and deliberate processing of the functional manipulability of objects. *Frontiers in Human Neuroscience*, 10, 360. <https://doi.org/10.3389/fnhum.2016.00360>
- Mizelle, J. C., Kelly, R. L., & Wheaton, L. A. (2013). Ventral encoding of functional affordances: A neural pathway for identifying errors in action. *Brain and Cognition*, 82(3), 274–282. <https://doi.org/10.1016/j.bandc.2013.05.002>
- Murray, S. O., Boyaci, H., & Kersten, D. (2006). The representation of perceived angular size in human primary visual cortex. *Nature Neuroscience*, 9(3), 429–434. <https://doi.org/10.1038/nn1641>
- Pelli, D. G. (1997). The VideoToolbox software for visual psychophysics: Transforming numbers into movies. *Spatial Vision*, 10(4), 437–442. <https://doi.org/10.1163/156856897X00366>
- Plewan, T., Weidner, R., Eickhoff, S. B., & Fink, G. R. (2012). Ventral and dorsal stream interactions during the perception of the Müller-Lyer illusion: Evidence derived from fMRI and Dynamic Causal Modeling. *Journal of Cognitive Neuroscience*, 24(10), 2015–2029. https://doi.org/10.1162/jocn_a_00258
- Pooresmaeli, A., Arrighi, R., Biagi, L., & Morrone, M. C. (2013). Blood oxygen level-dependent activation of the primary visual cortex predicts size adaptation illusion. *Journal of Neuroscience*, 33(40), 15999–16008. <https://doi.org/10.1523/JNEUROSCI.1770-13.2013>
- Riddoch, M. J., Humphreys, G. W., Edwards, S., Baker, T., & Willson, K. (2003). Seeing the action: Neuropsychological evidence for action-based effects on object selection. *Nature Neuroscience*, 6(1), 82–89. <https://doi.org/10.1038/nn984>
- Roberts, K. L., & Humphreys, G. W. (2010). Action relationships concatenate representations of separate objects in the ventral visual system. *Neuroimage*, 52(4), 1541–1548. <https://doi.org/10.1016/j.neuroimage.2010.05.044>
- Roberts, K. L., & Humphreys, G. W. (2011). Action relations facilitate the identification of briefly-presented objects. *Attention Perception & Psychophysics*, 73(2), 597–612. <https://doi.org/10.3758/s13414-010-0043-0>
- Salmon, J. P., McMullen, P. A., & Filliter, J. H. (2010). Norms for two types of manipulability (graspability and functional usage), familiarity, and age of acquisition for 320 photographs of objects. *Behavior Research Methods*, 42(1), 82–95. <https://doi.org/10.3758/BRM.42.1.82>
- Schwarzkopf, D. S., Song, C., & Rees, G. (2011). The surface area of human V1 predicts the subjective experience of object size. *Nature Neuroscience*, 14(1), 28–30. <https://doi.org/10.1038/nn.2706>
- Sim, E.-J., Helbig, H. B., Graf, M., & Kiefer, M. (2015). When action observation facilitates visual perception: Activation in visuo-motor areas contributes to object recognition. *Cerebral Cortex*, 25(9), 2907–2918. <https://doi.org/10.1093/cercor/bhu087>
- Smeets, J. B. J., & Brenner, E. (2019). Some illusions are more inconsistent than others. *Perception*, 48(7), 638–641. <https://doi.org/10.1177/0301006619853147>
- Smeets, J. B. J., Brenner, E., de Grave, D. D., & Cuijpers, R. H. (2002). Illusions in action: Consequences of inconsistent processing of spatial attributes. *Experimental Brain Research*, 147(2), 135–144. <https://doi.org/10.1007/s00221-002-1185-7>
- Smeets, J. B. J., Kleijn, E., van der Meijden, M., & Brenner, E. (2020). Why some size illusions affect grip aperture. *Experimental Brain Research*, 238(4), 969–979. <https://doi.org/10.1007/s00221-020-05775-1>
- Song, C., Sandberg, K., Andersen, L. M., Blicher, J. U., & Rees, G. (2017). Human occipital and parietal GABA selectively influence visual perception of orientation and size. *Journal of Neuroscience*, 37(37), 8929–8937. <https://doi.org/10.1523/jneurosci.3945-16.2017>
- Styrkowiec, P. P., Nowik, A. M., & Króliczak, G. (2019). The neural underpinnings of haptically guided functional grasping of tools: An fMRI study. *Neuroimage*, 194, 149–162. <https://doi.org/10.1016/j.neuroimage.2019.03.043>

- Tettamanti, M., Conca, F., Falini, A., & Perani, D. (2017). Unaware processing of tools in the neural system for object-directed action representation. *Journal of Neuroscience*, 37(44), 10712–10724. <https://doi.org/10.1523/jneurosci.1061-17.2017>
- Tucker, M., & Ellis, R. (1998). On the relations between seen objects and components of potential actions. *Journal of Experimental Psychology. Human Perception and Performance*, 24(3), 830. <https://doi.org/10.1037/0096-1523.24.3.830>
- Van de Steen, F., Krebs, R. M., Colenbier, N., Almgren, H., & Marinazzo, D. (2020). Effective connectivity modulations related to win and loss outcomes. *Neuroimage*, 207, 116369. <https://doi.org/10.1016/j.neuroimage.2019.116369>
- Van Elk, M., & Blanke, O. (2011). Manipulable objects facilitate cross-modal integration in peripersonal space. *Plos One*, 6(9), Article e24641. <https://doi.org/10.1371/journal.pone.0024641>
- Wang, A., Chen, L., & Jiang, Y. (2021). Anodal occipital transcranial direct current stimulation enhances perceived visual size illusions. *Journal of Cognitive Neuroscience*, 33(3), 528–535. https://doi.org/10.1162/jocn_a_01664
- Weidner, R., Plewan, T., Chen, Q., Buchner, A., Weiss, P. H., & Fink, G. R. (2014). The moon illusion and size-distance scaling-evidence for shared neural patterns. *Journal of Cognitive Neuroscience*, 26(8), 1871–1882. https://doi.org/10.1162/jocn_a_00590
- Yang, H., He, C., Han, Z., & Bi, Y. (2020). Domain-specific functional coupling between dorsal and ventral systems during action perception. *Scientific Reports*, 10(1), 21200. <https://doi.org/10.1038/s41598-020-78276-4>
- Zeidman, P., Jafarian, A., Corbin, N., Seghier, M. L., Razi, A., Price, C. J., et al. (2019). A guide to group effective connectivity analysis, part 1: First level analysis with DCM for fMRI. *Neuroimage*, 200, 174–190. <https://doi.org/10.1016/j.neuroimage.2019.06.031>